10.1109/ULTSYM.2013.0107

Modeling volume power spectra for collections of spheres in a finite container

Adam C. Luchies and Michael L. Oelze
Bioacoustics Research Laboratory, Department of Electrical and Computer Engineering
University of Illinois at Urbana-Champaign
Urbana, Illinois, 61820
Email: oelze@illinois.edu

***Abstract*—When modeling the volume power spectrum for a collection of randomly positioned scatterers in an impedance map, the assumption is usually made that the incoherent component of the spectrum is much larger than the coherent component. With this assumption, scattering form-factor models such as the Gaussian, fluid-filled sphere, etc. can be fitted to the impedance map volume power spectrum for the purpose of estimating parameters such as the scatterer size. The accuracy of the assumption concerning incoherent and coherent component spectrum magnitudes was studied using simulated collections of spheres in a finite container.**

A collection of spheres with a specific number density was simulated and the volume power spectrum was computed by taking the 3D Fourier Transform and squaring the modulus. Realizations of spheres with random positions within a cubical or spherical container were simulated and the resulting volume power spectra were averaged to study the expected value of the power spectrum versus different number densities of spheres. These results were compared to the volume power spectrum for a single sphere (i.e., the fluid-filled sphere form factor). A single sphere volume power spectrum is expected if no coherent component in the spectrum exists.

For low number density, the volume power spectrum for a collection of spheres matched the single sphere power spectrum. As volume fraction increased, the volume power spectrum became biased for low values of *ka* compared to the power spectrum for a single sphere. The source of this bias can be attributed to the interaction of sphere positions. As more spheres are placed in the container, their positions become less random, increasing the effect of the coherent component relative to the incoherent component. The simulations also indicated that the container shape affected the shape of the volume spectrum. When using a cube as the container for the collection of spheres, asymmetry was observed in the volume power spectrum. Specifically, peaks were present on-axis in *k*-space that were not present off-axis nor in the power spectrum for a single sphere. When changing the container to a sphere, the volume power spectrum was symmetric and the on-axis peaks observed for the cube container were not present.

The results of this study indicate that when modeling the effects of scattering using single scattering approximations, a large number density may yield a significant coherent component in the power spectrum and the shape of the scattering volume must be taken into account.

This work was supported by NIH Grant R01-EB008992.

I. Introduction

Quantitative ultrasound parameters have shown significant promise for diagnosing disease in the human body [1], [2]. Spectral-based parameters, such as the spectral slope, spectral intercept, ESD, EAC, and BSC utilize information in the backscatter signal to estimate localized information about the structure and geometry of acoustic impedance values in tissue. The acoustic impedance map is a computational tool designed to study the available information from the frequency content of ultrasonic backscattered signals. By relating the volume power spectrum of an impedance map to ultrasonic backscatter from the tissue, spectral based ultrasound parameters can be studied computationally [3], [4]. Once the volume power spectrum has been estimated from an impedance map, it can be modeled by the power spectrum for a volume containing a single scatterer. Modeling in this manner requires the assumption that the incoherent term of the power spectrum dominates the coherent term. The goal of this work is to examine this assumption using simulations of collections of spheres in a finite container.

II. Methods

A. Modeling a Collection of Monodisperse Spheres

A collection of monodisperse (uniform size) spheres in n-dimensions may be described mathematically in the following way. A single sphere centered at the origin is written as

$$h(\mathbf{r}) = \begin{cases} 1, \mathbf{r} \leq a \\ 0, \mathbf{r} > a \end{cases} \tag{1}$$

where a is the spherical radius and $\mathbf{r} \in \mathrm{R}^n$. The spatial positions of each sphere are given by

$$f(\mathbf{r}) = \sum_{n=1}^{N} \delta(\mathbf{r} - \mathbf{r}_i) \tag{2}$$

where δ is the Dirac delta function, N is the total number of spheres in the collection, and $\mathbf{r}_i$ records the position of the ith sphere. The collection of spheres is written as

$$s(\mathbf{r}) = h * f \tag{3}$$

where * indicates spatial convolution. The volume power spectrum for the collection of spheres is given by

$$|S(\mathbf{k})|^2 = |H(\mathbf{k})|^2 |F(\mathbf{k})|^2 \tag{4}$$

TABLE I. SPHERE FOURIER TRANSFORMS IN DIFFERENT DIMENSIONS.

n	1	2	3
$H(ka)$	$j_0(ka)$	$2\frac{J_1(ka)}{ka}$	$3\frac{j_1(ka)}{ka}$

where $\mathbf{k}$ is the wavenumber vector, $F(\mathbf{k})$ is the Fourier transform of $f(\mathbf{r})$, and $H(\mathbf{k})$ is the Fourier transform of $h(\mathbf{r})$. For a collection of monodisperse spheres with known radius, $H(\mathbf{k})$ is deterministic and depends on the number of dimensions and the sphere radius as shown in Table I.

The power spectrum for $f(\mathbf{r})$ can be written as

$$|F(\mathbf{k})|^2 = N + 2\sum_{i<k} \cos(\mathbf{k}\cdot\Delta_{i,j}) \tag{5}$$

where $\Delta_{i,k} = \mathbf{r}_i - \mathbf{r}_k$ is the spacing vector between the ith and kth spheres. If the positions of the spheres are random, $|F(\mathbf{k})|^2$ is a random function of the wavenumber vector. The first addend in Eqn. 5 is called the incoherent component and the second is called the coherent term. If the spheres are located randomly, it is often assumed that the incoherent term dominates compared to the coherent term, allowing the spectrum for the collection of spheres to be written as

$$|S(\mathbf{k})|^2 = N\,|H(\mathbf{k})|^2\,. \tag{6}$$

If this assumption is true, the spectrum for the collection of spheres can be modeled by the spectrum for a volume containing a single sphere and scaled by the total number of spheres in the collection.

B. Random Sequential Absorption

Monodisperse hard spheres (spheres were not allowed to overlap) were simulated in finite containers for one-, two-, and three dimensional collections and for different volume fractions. A sphere location configuration was generated using a random sequential absorption process (RSA). A random position was selected in the container and a sphere was placed in this position as long as it did not overlap any existing spheres in the container. This process was repeated until the desired number of spheres filled the container. For the one-dimensional simulations, the line container had length of 1.0 and the spheres were simulated with radius $a = 0.001$. For the two-dimensional simulations, the square container had side length of 1.0 and the spheres were simulated with radius $a = 0.025$. Initial results indicated that the container shape plays a role in the expected power spectrum for a collection of spheres, so collections of spheres in a circle container with diameter 1.0 were also studied. For the three-dimensional simulations, the cubical container had side length of 1.0, the spherical container had diameter 1.0, and the spheres were simulated with radius $a = 0.2$. For each sphere configuration, a volume with specified sampling rate was created. A total of 10^4 sampling points were used for the one-dimensional simulations and 10^3 sampling points were used along each dimension for the two- and three-dimensional simulations. The impedance value of the volume was set to 1.0 for sampling points that were inside a sphere and the impedance value was set to 0.0 for sampling points that were not inside any spheres.

III. AVERAGED POWER SPECTRA FOR COLLECTIONS OF SPHERES

For the one-dimensional simulations, 250 random sphere configurations were generated. For each configuration, a volume containing the spheres was generated and the power spectral estimate was made using the squared modulus of the Fourier transform. The spectra were averaged and normalized to intersect the $ka = 0$ axis at 1.0. Results can be seen in Figure 1.

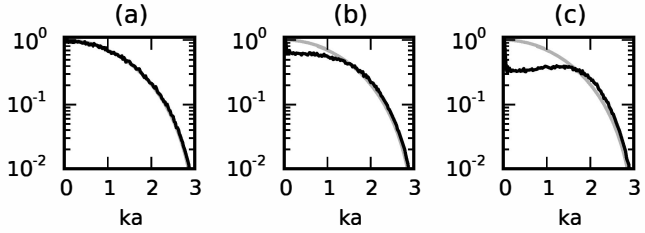

Fig. 1. Averaged power spectra for one-dimensional collections of spheres for (a) 2%, (b) 20%, and (c) 40% volume fractions. The spectrum for a single sphere is shown in light gray.

For the two-dimensional simulations, 250 random sphere configurations were generated. For each configuration, a volume containing the spheres was generated and the power spectral estimate was made using the squared modulus of the Fourier transform. The spectra were averaged and normalized to intersect the $ka = 0$ axis at 1.0. Results when using a square container in Figure 2 and when using a circle container in Figure 3.

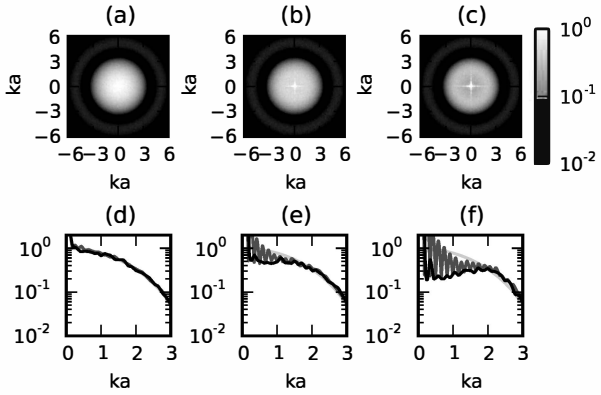

Fig. 2. Averaged power spectra for two-dimensional collections of spheres in a square container for (a) 1%, (b) 15%, and (c) 30% volume fractions. Radial line samples from the averaged power spectra in (a-c) for $\theta = 0°$ (gray) and $\theta = 45°$ (black) for (e) 1%, (e) 15%, and (f) 30% volume fractions. The spectrum for a single sphere is shown in light gray.

For the three-dimensional simulations, 250 random sphere configurations were generated. For each configuration, a volume containing the spheres was generated and the power spectral estimate was made using the squared modulus of the Fourier transform. The spectra were averaged and normalized to intersect the $ka = 0$ axis at 1.0. Results when using a cube container are shown in Figure 4 and when using a sphere container in Figure 5.

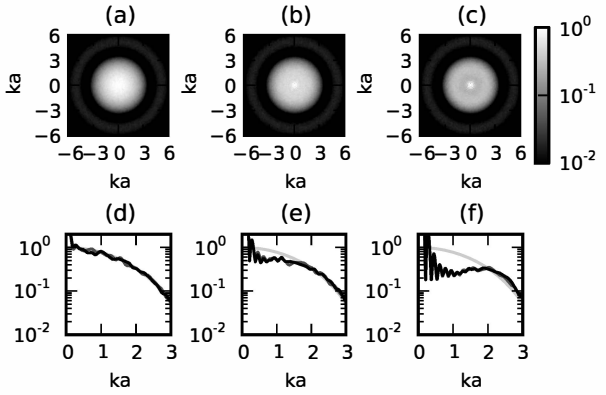

Fig. 3. Averaged power spectra for two-dimensional collections of spheres in a circle container for (a) 1%, (b) 15%, and (c) 30% volume fractions. Radial line samples from the averaged power spectra in (a-c) for $\theta = 0^\circ$ (gray) and $\theta = 45^\circ$ (black) for (d) 1%, (e) 15%, and (f) 30% volume fractions. The spectrum for a single sphere is shown in light gray.

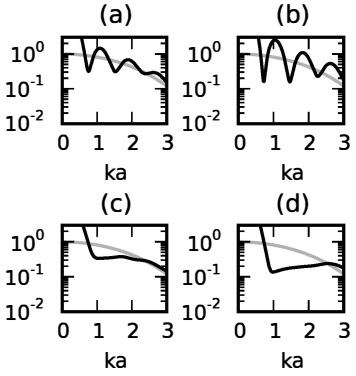

Fig. 4. Radial line samples from averaged power spectra for three-dimensional collections of spheres in a cube container for (a, c) 8% and (b, d) 16% volume fractions. Radial lines were sampled at (a, b) $\theta = 0^\circ, \phi = 0^\circ$ and (c, d) $\theta = 45^\circ, \phi = 45^\circ$.

IV. Power Spectral Modeling for a Collection of Spheres

By modeling the randomness of the spacings in Eqn. 5, a model can be created for the observed spectral estimates. Bringing the expectation on the inside of the summation for Eqn. 5 provides an expression for the expected value of the sphere position power spectrum.

$$E\left\{\left|F(\mathbf{k})\right|^2\right\} = N + 2\sum_{i<k} E\left\{\cos(\mathbf{k}\cdot\Delta_{i,k}\right\}. \tag{7}$$

The expected value can then be evaluated assuming that only two spheres are located in the medium, resulting in the following expression

$$|S(\mathbf{k})|^2_{modeled} = \frac{|H(\mathbf{k})|^2}{N}\left[N + N(N-1)E\left\{\cos(\mathbf{k}\cdot\Delta\right\}\right]. \tag{8}$$

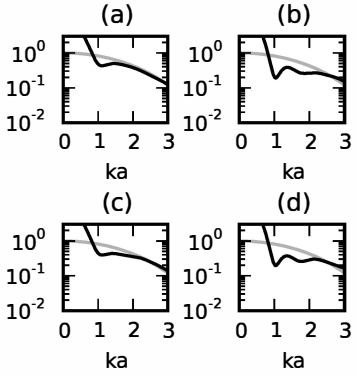

Fig. 5. Radial line samples from averaged power spectra for three-dimensional collections of spheres in a sphere container for (a, c) 8% and (b, d) 16% volume fractions. Radial lines were sampled at (a, b) $\theta = 0^\circ, \phi = 0^\circ$ and (c, d) $\theta = 45^\circ, \phi = 45^\circ$.

In order to evaluate the $E\left\{\cos(\mathbf{k}\cdot\Delta)\right\}$ term, a distribution for the spacings is needed. In one-dimension, the non-overlapping behavior was captured using a gapped triangle distribution given by

$$p(\Delta) = \begin{cases} \frac{L-\Delta}{L-2a}, & |\Delta| \in [2, L] \\ 0, & \text{else} \end{cases} \tag{9}$$

where L is the length of the container. The gapped triangle distribution was extended to two- and three-dimensions for cubical and spherical containers.

V. Modeling Results

In the figures below, modeled power spectra for one-, two-, and three-dimensions for various volume fractions are displayed in gray. For comparison, the results for the averaged power spectra from simulated collections of spheres as shown in Figs. 1-5 are displayed in black. The modeled and averaged spectra are very similar, with the fit degrading for higher volume fractions. The results for one-dimensions are shown in Figure 6.

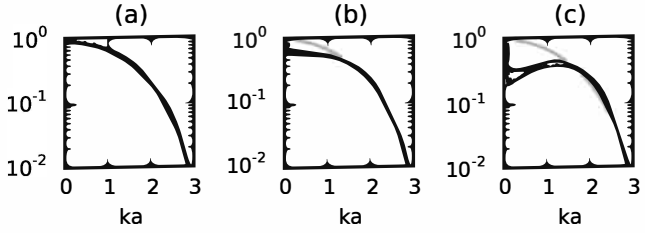

Fig. 6. Modeled (gray) and averaged (black) power spectrum for one-dimensional collections of spheres for (a) 2%, (b) 20%, and (c) 40% volume fractions. The spectrum for a single sphere is shown in light gray.

The results for two-dimensions when using a square container are shown in Figure 7 and when using a circle container in Figure 8. The results for three-dimensions when using a cube container are shown in Figure 9 and when using a sphere container in Figure 10.

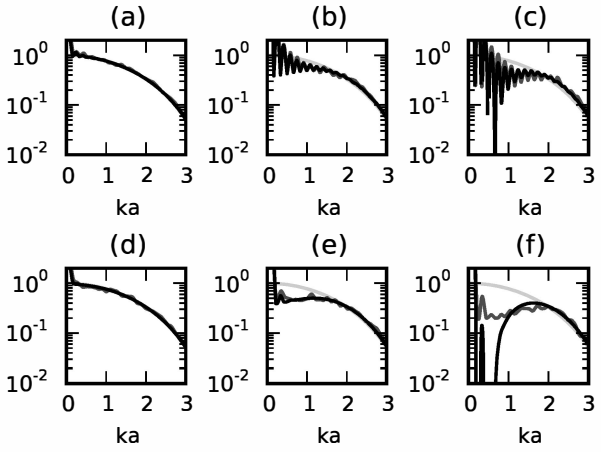

Fig. 7. Radial line samples for modeled (gray) and averaged (black) power spectra for two-dimensional collections of spheres in a square container for (a, d) 1%, (b, e) 15%, and (c, f) 30% volume fractions sampled (a-c) $\theta = 0°$ and (d-f) $\theta = 45°$ The spectrum for a single sphere is shown in light gray.

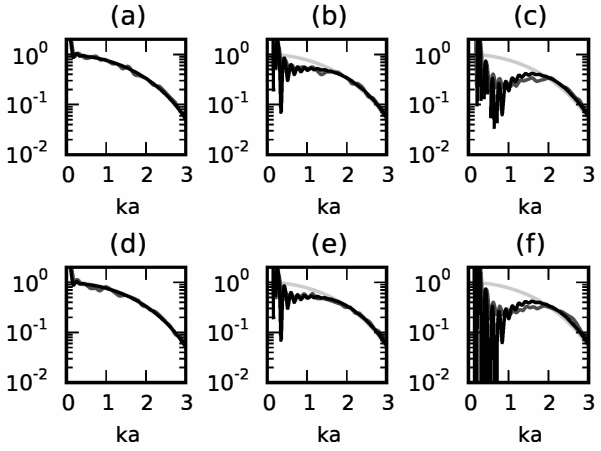

Fig. 8. Radial line samples for modeled (gray) and averaged (black) power spectra for two-dimensional collections of spheres in a circle container for (a, d) 1%, (b, e) 15%, and (c, f) 30% volume fractions sampled (a-c) $\theta = 0°$ and (d-f) $\theta = 45°$ The spectrum for a single sphere is shown in light gray.

VI. Conclusion

The results suggest two important features related to power spectral estimates from impedance maps. When computing the power spectrum from an acoustic impedance map using the squared modulus of the three-dimensional Fourier transform, the power spectral shape is affected by the spacings between the scatterers and by the container shape. The spherical container shape provides estimates that are symmetric in all *k*-space directions. In the case of an impedance map, the probability of scatterer overlap is zero, while for the case of an ultrasonic scan, the probability of scatterer overlap is non-zero (e.g., as shown in Fig. 11, two scatterers located at the same depth, but different lateral positions). The gap pattern created by the nonoverlapping scatterer condition results in deviations of the power spectrum from the theoretical. Therefore, in processing impedance maps, techniques must be used that allow the effects of scatterer overlap.

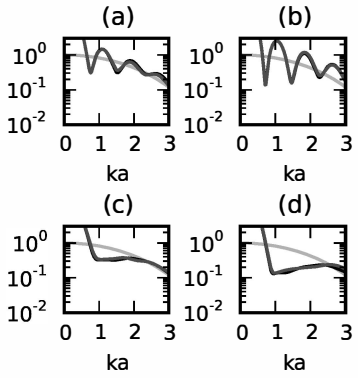

Fig. 9. Radial line samples of modeled (gray) and averaged (black) samples from averaged power spectra for three-dimensional collections of spheres in a cube container for (a, c) 8% and (b, d) 16% volume fractions. Radial lines were sampled at (a, b) $\theta = 0°, \phi = 0°$ and (c, d) $\theta = 45°, \phi = 45°$. The spectrum for a single sphere is shown in light gray.

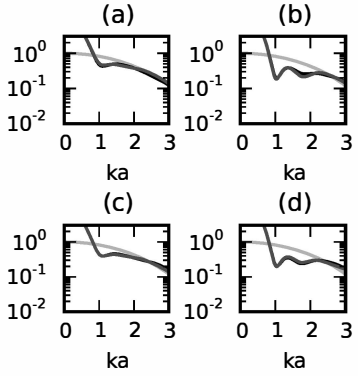

Fig. 10. Radial line samples of modeled (gray) and averaged (black) samples from averaged power spectra for three-dimensional collections of spheres in a sphere container for (a, c) 8% and (b, d) 16% volume fractions. Radial lines were sampled at (a, b) $\theta = 0°, \phi = 0°$ and (c, d) $\theta = 45°, \phi = 45°$. The spectrum for a single sphere is shown in light gray.

References

[1] F. L. Lizzi, M. Greenebaum, E. J. Feleppa, M. Elbaum, and D. J. Coleman. Theoretical framework for spectrum analysis in ultrasonic tissue characterization. *J. Acoust. Soc. Am.*, vol. 73, p. 1366, 1983.

[2] M. F. Insana, R. F. Wagner, D. G. Brown, and T. J. Hall. Describing small-scale structure in random media using pulse-echo ultrasound. *J. Acoust. Soc. Am.*, vol. 87, p. 179, 1990.

[3] J. Mamou, M. L. Oelze, W. D. O'Brien Jr, and J. F. Zachary. Identifying ultrasonic scattering sites from three-dimensional impedance maps. *J. Acoust. Soc. Am.*, vol. 117, p. 413, 2005.

[4] A. J. Dapore, M. R. King, J. Harter, S. Sarwate, M. L. Oelze, J. A. Zagzebski, M. N. Do, T. J. Hall, and W. D. O'Brien. Analysis of human fibroadenomas using three-dimensional impedance maps. *IEEE Trans. on Med. Imag.*, vol. 30, p. 1206, 2011.

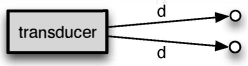

Fig. 11. The two objects are at different positions in space, but they appear to be at the same position to the transducer.